The Astrophysical Journal Letters, 933:L28 (6pp), 2022 July 10 https://doi.org/10.3847/2041-8213/ac7c0b

Tidal Disruption on Stellar-mass Black Holes in Active Galactic Nuclei

Y. Yang[1], I. Bartos[1], G. Fragione[2,3], Z. Haiman[4], M. Kowalski[5,6], S. Márka[7], R. Perna[8,9], and H. Tagawa[10]
[1] Department of Physics, University of Florida, PO Box 118440, Gainesville, FL 32611-8440, USA
[2] Department of Physics & Astronomy, Northwestern University, Evanston, IL 60208, USA; imrebartos@ufl.edu
[3] Center for Interdisciplinary Exploration & Research in Astrophysics (CIERA), Northwestern University, Evanston, IL 60208, USA
[4] Department of Astronomy, Columbia University, 550 W. 120th Street, New York, NY 10027, USA
[5] Deutsches Elektronen Synchrotron DESY, Platanenallee 6, D-15738 Zeuthen, Germany
[6] Institut fur Physik, Humboldt-Universit at zu Berlin, D-12489 Berlin, Germany
[7] Columbia Astrophysics Laboratory, Columbia University in the City of New York, New York, NY 10027, USA
[8] Department of Physics and Astronomy, Stony Brook University, Stony Brook, NY 11794-3800, USA
[9] Center for Computational Astrophysics, Flatiron Institute, New York, NY 10010, USA
[10] Astronomical Institute, Graduate School of Science, Tohoku University, Aoba, Sendai 980-8578, Japan
Received 2021 December 3; revised 2022 June 23; accepted 2022 June 26; published 2022 July 7

Abstract

Active galactic nuclei (AGNs) can funnel stars and stellar remnants from the vicinity of the galactic center into the inner plane of the AGN disk. Stars reaching this inner region can be tidally disrupted by the stellar-mass black holes in the disk. Such micro tidal disruption events (micro-TDEs) could be a useful probe of stellar interaction with the AGN disk. We find that micro-TDEs in AGNs occur at a rate of $\sim 170\,\mathrm{Gpc}^{-3}\ \mathrm{yr}^{-1}$. Their cleanest observational probe may be the electromagnetic detection of tidal disruption in AGNs by heavy supermassive black holes ($M_\bullet \gtrsim 10^8\,M_\odot$) that cannot tidally disrupt solar-type stars. The reconstructed rate of such events from observations, nonetheless, appears to be much lower than our estimated micro-TDE rate. We discuss two such micro-TDE candidates observed to date (ASASSN-15lh and ZTF19aailpwl).

Unified Astronomy Thesaurus concepts: Tidal disruption (1696); Active galaxies (17)

1. Introduction

A few percent of galaxies host a central, compact, highly luminous region called the active galactic nucleus (AGN). AGNs are the result of a highly accreting supermassive black hole (SMBH), in which infalling gas forms an accretion disk around the SMBH.

In addition to being the source of the high central luminosity, AGN disks can also impact the dynamics of stellar remnants in the galactic center. Of particular interest has been the interaction of AGN disks with stellar-mass black holes (BHs) that have migrated to the galactic center through mass segregation (Alexander & Hopman 2009; Keshet et al. 2009). While orbiting the central SMBH, BHs periodically cross the AGN disk that gradually aligns their orbit with the disk plane (Bartos et al. 2017). Once in the plane, BHs migrate inwards due to viscous tidal interactions with the disk (Levin 2007; McKernan et al. 2012). If these processes bring two BHs into each others' vicinity, the dense gas of the AGN disk facilitates gravitational capture and ultimately their merger through dynamical friction.

BH mergers in AGN disks may be an important gravitational-wave source with BH properties distinct from those expected from other astrophysical mechanisms (Bartos et al. 2017; Stone et al. 2017; McKernan et al. 2018; Secunda et al. 2019; Yang et al. 2019a; Tagawa et al. 2020b). Merging BHs or neutron stars in AGN disks might also produce detectable electromagnetic emission, opening up another way to study AGN-assisted mergers (McKernan et al. 2019; Kimura et al. 2021; Perna et al. 2021a, 2021b; Zhu et al. 2021).

Stellar orbits are also affected by AGN disks as disk crossings dissipate orbital energy (Miralda-Escudé & Gould 2000; Panamarev et al. 2018), which will be particularly significant for stars on highly eccentric orbits. Some of these stars will gradually get closer to the central SMBH until they are tidally disrupted by it. Nonetheless, such interactions with the AGN disk may have limited effect on the overall tidal disruption rate in galaxies with AGNs (Kennedy et al. 2016; MacLeod & Lin 2020, but see Tadhunter et al. 2017; Pan & Yang 2021).

Here we examine the orbital alignment of stars with the AGN disk and its consequences. Similarly to BHs and neutron stars, some of the stars in galactic centers will align their orbits with the AGN disk plane. Once in the plane, stars can form binaries with BHs, leading to their eventual tidal disruption within the AGN disk (Section 2). Such "micro" tidal disruption events around BHs (hereafter micro-TDEs; Perets et al. 2016) might have different radiation features than standard TDEs around SMBHs in particular in the X-ray and gamma-ray band (Section 3). We argue that AGNs around the heaviest SMBHs may be the best location for identifying micro-TDEs as these SMBHs cannot disrupt solar-type stars (Section 4). We estimate the rate density of micro-TDEs in AGNs in Section 2.5 and present our conclusions in Section 5.

2. Binary Formation, Evolution, and Tidal Disruption

In this section we describe our computation of the occurrence of tidal disruptions starting from an initial system including a central supermassive BH with an accretion disk surrounded by stars and stellar remnants.

2.1. Initial Conditions

We considered stars and stellar remnants that initially orbit the galactic nucleus as single objects. Stars were considered to

be main sequence. Their evolution due to fusion was ignored over the period of the AGN activity; however, their mass could change due to accretion from the AGN disk (Cantiello et al. 2021; Dittmann et al. 2021; Jermyn et al. 2021).

We considered the AGN disk to be geometrically thin, optically thick, radiatively efficient, steady state (Shakura & Sunyaev 1973), but self-gravitating (Sirko & Goodman 2003). We adopted the viscosity parameter $\alpha = 0.1$, accretion rate $\dot{M}_{\bullet} = 0.1\dot{M}_{\rm Edd}$, and radiation efficiency $\epsilon = 0.1$. We used a fiducial SMBH mass of $10^6\,M_{\odot}$. We expect the results to be weakly dependent on this choice (Yang et al. 2019b), which we confirm below by a comparison study with an SMBH mass of $10^8\,M_{\odot}$.

We assumed that the stars follow a mass–radius relation $R_* = 1.06(M_*/{\rm M}_{\odot})^{0.945}$ for $M_* < 1.66M_{\odot}$ and $1.33(M_*/{\rm M}_{\odot})^{0.555}$ for $M_* > 1.66M_{\odot}$ (Demircan & Kahraman 1991). We assumed that the stellar mass follows a Kroupa initial mass function (Kroupa 2001). We took into account the mass segregation in the spatial distributions of main-sequence stars, adopting $dN/da \propto a^{-3/2-0.5M_*/M_{\rm max}}$, where a is the semimajor axes of the star's orbit around the SMBH (Keshet et al. 2009; Alexander & Hopman 2009; Gondán et al. 2018). In the subsequent evolution, we ignore the effect of dynamical relaxation processes outside the AGN disk as they are generally relevant on a much longer timescale than the AGN-assisted orbital evolution considered here for the objects that will merge within the AGN lifetime (Kocsis & Tremaine 2011; Alexander 2017).

The stars had an initially uniform eccentricity distribution and isotropic directional distribution. We adopted a maximum stellar mass of $M_{\rm max} = 50\,M_{\odot}$, which accounts for the fact that the lifetime of the most massive stars is too short for them to participate in mass segregation. The total stellar mass within the gravitational influence radius of the SMBH was taken to be equal to the mass of the SMBH (Miralda-Escudé & Gould 2000).

For simplicity, we adopted the Salpeter initial mass function $dN/dM \propto M^{-2.35}$ for BHs within the range of 5–50 $M_{\odot}$ and a normal initial mass function $M/M_{\odot} \sim N(1.49, 0.19)$ for neutron stars (Özel & Freire 2016). We assumed that the total mass of the BH population is 1.6% of the stellar mass in galactic centers and the number of neutron stars is 10 times the number of BHs (Gondán et al. 2018). This ratio is consistent with expectations from our assumed Kroupa stellar-mass distribution. We took into account mass segregation following Gondán et al. (2018).

2.2. Orbital Alignment with the AGN Disk

The first step in the process is the orbital alignment of some of the stars and stellar remnants in the galactic center with the plane of the AGN disk. Every time a star or stellar remnant crosses the AGN disk, its velocity changes due to the accretion of matter from the disk. We simulated the resulting orbital evolution following Yang et al. (2019b). The mass of infalling gas upon each crossing is given by $\Delta m_{\rm gas} = v_{\rm rel}\,t_{\rm cross}\,R_{\rm cap}^2\,\pi\Sigma/(2H)$, $R_{\rm cap} = \max\{R, R_{\rm BHL}\}$, $R_{\rm BHL} \equiv 2GM/(v_{\rm rel}^2 + c_s^2)$ is the stars' Bondi–Hoyle–Lyttleton radius, c_s is the speed of sound, R and M are the objects radius and mass, respectively, Σ and H are the surface density and scale height of the AGN disk, respectively, $t_{\rm cross} \equiv 2H/v_z$ is the crossing time, and v_z is the z component of the stars' velocity. Mass loss by a main-sequence star due to the ram pressure exerted by the disk gas is negligible (Miralda-Escudé & Kollmeier 2005).

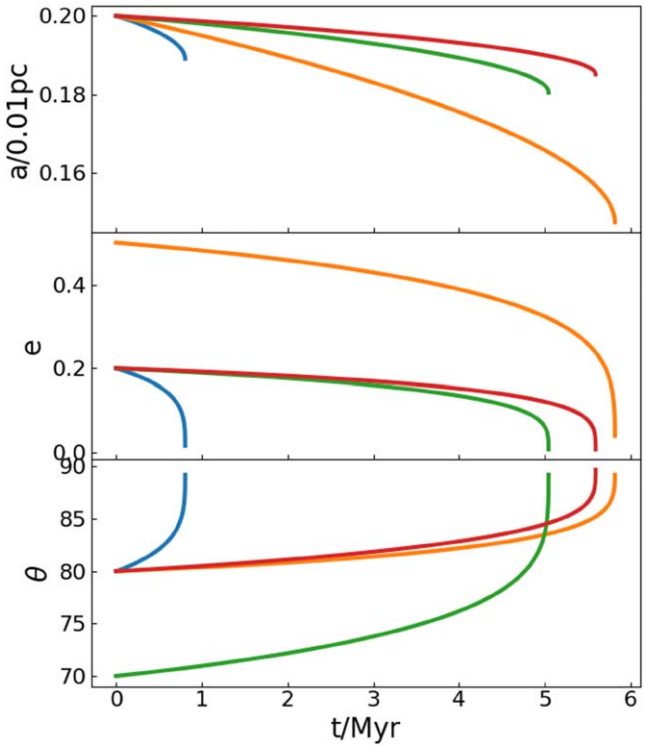

Figure 1. Example evolution of orbital parameters. Evolution is shown as a function of time for the semimajor axis a (top), eccentricity e (middle), and inclination θ (angle between the semimajor axis and the AGN disk plane in degrees; bottom) for four sample orbits. Each example orbit begins with $a = 0.02$ pc and has the following initial parameters. Blue: $e = 0.2$, $\theta = 80°$, $\psi = 0°$. Orange: $e = 0.5$, $\theta = 80°$, $\psi = 0°$. Green: $e = 0.2$, $\theta = 70°$, $\psi = 0°$. Red: $e = 0.2$, $\theta = 80°$, $\psi = 20°$. Here, ψ is the initial angular rotation of the semiminor axis from the disk plane; see Yang et al. (2019b).

We computed the changes in the velocity and angular momentum of the star upon each crossing based on momentum conservation. We updated orbital parameters after each crossing according to the change of velocity and hence obtained the orbital evolution iteratively. Four illustrative examples of orbital parameter evolutions are shown in Figure 1.

2.3. Binary Formation within the Accretion Disk

Once some of the stars and stellar remnants are embedded in the AGN disk, they begin migrating inward. We adopted the type I and type II migration rates given in Tagawa et al. (2020a), accounting for the possibility of gap opening in the disk. We ignored any effect on migration by disk formation around stars or stellar remnants. We assumed that stars and stellar remnants similarly migrate inwards within the AGN disk. Both orbital alignment and migration increase the number density of each type of object in the inner AGN disk, leading to efficient binary formation through gravitational capture (Tagawa et al. 2020b). Dynamical friction within the gas further facilitates the formation of binaries and their consecutive hardening. For the system parameters considered here, binary–single and binary–binary interactions did not significantly affect the resulting mergers (Gayathri et al. 2021), resulting in the object's migration to a central migration trap at a distance of about 300 Schwarzschild radii from the central supermassive BH (Bellovary et al. 2016). As binary inspiral is expected to be fast compared to the AGN lifetime, we assumed that nearby objects in the disk form binaries without simulating

the process itself. We considered two objects "nearby" once both of them approached the migration trap to within their Hill radius. The remnant following any merger was considered to be a BH.

2.4. Star–Black Hole Binaries

Let us consider a binary consisting of a main-sequence star and a BH. The binary typically forms at small separations of only $\sim$10 times the star's tidal radius $R_t = R_*(M_{bh}/M_*)^{1/3}$ and could be eccentric at (or soon after) its birth, either due to its formation (see Funato et al. 2004) and/or subsequently driven to be eccentric by a circumbinary disk (D'Orazio & Duffell 2021; Zrake et al. 2021). This could justify an impulsive disruption "event" at the pericenter of an ellipse, rather than a slow circular inspiral and gradual tidal "peeling" (MacLeod et al. 2013).

Once the binary's pericenter distance R_p approaches R_t, the star is tidally disrupted. TDEs around SMBHs typically occur at parabolic ($e \approx 1$) stellar orbits, leading to a tidal tail that will affect long-term accretion. In addition, partial disruption has a substantially larger cross section in the case of TDEs and should be more common (Stone et al. 2020).

2.5. Expected Rate Density of Micro-TDEs

The rate density of micro-TDEs depends on the random process of alignment of stars and stellar remnants. First, as the expected number of alignments is small, it will randomly fluctuate from galaxy to galaxy. Second, the random order in which stars and stellar remnants align will determine the type of the ultimate event.

To account for this random process, we first computed the average number of stars, BHs, and neutron stars that undergo orbital alignment with the AGN disk within the AGN's lifetime (assumed to be 10^7 yr) using the initial conditions and evolution described above. We found an expected $\sim$5 orbital alignments for BHs and neutron stars and $\sim$100 alignments for stars (see also Yang et al. 2020). We assumed for simplicity that the expected rate of orbital alignment is identical in every AGN (there is only a weak dependence on the AGN properties; Yang et al. 2019b). For comparison, assuming an SMBH mass of $10^8\,M_\odot$, we obtain an expected 3, 2, and 100 alignments for BHs, neutron stars, and stars, respectively.

Second, we carried out a Monte Carlo simulation to estimate the rate and type of mergers within AGNs by accounting for the random order of the alignments. In one realization, we randomly selected the number of stars, BHs, and neutron stars that align their orbit with the AGN disk. These numbers were drawn from a Poisson distribution around their expected values found above. For each object that aligns its orbit, we randomly selected their masses (and for the BHs, spins) from the underlying distributions we found for these objects within the disk. We then randomized the order of the objects and considered that they consecutively align their orbits with the AGN disk. Once in the disk, we considered that each object merges with the object already present in the disk (either the first object that aligned its orbit with the disk or the remnant of previous merger(s)).

With this approach, we ignored the possibility that some objects might not have time to migrate and merge, given that the characteristic migration time of $\lesssim$0.03 Myr for $M_\bullet \lesssim 10^8\,M_\odot$ (McKernan et al. 2020) is much less than the AGN lifetime. We also ignored that the order of mergers might be changed given the distribution of the initial radii of objects after alignment, as the characteristic migration time in the disk is less than the characteristic time between two alignments ($\sim$0.1 Myr^{-1}).

We carried out the above Monte Carlo realizations 10^4 times to obtain the expected fractions for the different types of mergers. We adopted an AGN number density $n_{AGN} = 0.018$ Mpc^{-3} (Hao et al. 2005) to obtain the corresponding rate densities. Table 1 shows the resulting expected merger and micro-TDE rate densities for all possible combinations of stars, BHs, and neutron stars. Given the size of our Monte Carlo study, these results have a $\sim$1% statistical error. Comparing our fiducial alignment rates with those for a $10^8\,M_\odot$ supermassive BH gives a systematic error on the order of 1% for our micro-TDE rate and up to a factor of 2 for the different merger types.

Table 1
Expected Rate Density of Binary Mergers/Disruptions in AGNs

	Black Hole	Neutron Star	Star
Black hole	13	1	170
Neutron star		10^{-3}	0.14
Star			20

Note. Micro-TDEs correspond to BH–star encounters. Results are shown in units of Gpc^{-3} yr^{-1} and have a statistical uncertainty of $\sim$1%. Most disrupted stars have masses $\lesssim 1\,M_\odot$, with about 10% having mass $>10\,M_\odot$. While BHs are the least common, they dominate the merger rate as their higher mass results in more efficient mass segregation and orbital alignment, while their mergers result in BHs that can undergo further mergers in the AGN disk.

3. Radiation Features of Micro-TDEs

While in some ways similar, TDE and micro-TDE light curves and spectra can differ due to multiple effects. An important feature that distinguishes them is the fact that, while cooling of the flow is efficient in TDEs, it is not in micro-TDEs, as shown by Wang et al. (2021). Hence, the flow is hotter and radiation pressure becomes important. Another interesting difference is in the fact that, due to the smaller mass of the BH in the micro-TDE case, there can be a kick to the BH due to the unbound mass from the disruption event itself (see also Kremer et al. 2022). We note that these kicks do not affect the overall micro-TDE rate as the kicked BHs in the inner regions are typically easily recaptured (Tagawa et al. 2020a).

Smoothed-particle hydrodynamics (SPH; Springel 2010) simulations with the `Phantom code` (Price et al. 2018), modified to allow for both the contribution of radiation pressure as well as for the center-of-mass motion of the BH+remnant system, were carried out by Wang et al. (2021) for a range of BH masses between 5 and $90\,M_\odot$. The general features are those of an optically thick remnant disk, larger and thicker than the one that forms in situations in which radiative cooling is efficient. Due to the large radiation pressure in the internal regions of the disk, some material is blown away. As typical for TDEs, the accretion rate was found to follow a power-law, with a mass-dependent index, varying from $t^{-5/3}$ to $t^{-9/4}$, with steeper indices corresponding to lower BH masses. Additionally, the simulations found that the self-gravity of the fallback stream causes the collapse of the disrupted material into small clumps before accreting onto the BH. In turn, these collapsed clumps cause the fallback rate to fluctuate. This can be of relevance to observational identifications of these events.

A further potential difference is that TDEs occur with highly eccentric orbits ($e \approx 1$), while AGN-assisted micro-TDEs may be less eccentric. For the latter, accretion may initially drive the binary to moderate eccentricity (Zrake et al. 2021), which subsequently can circularize due to gravitational-wave emission, except in rare multibody interactions (Samsing et al. 2022). Lower eccentricity could allow a larger fraction of the stellar matter to remain in the vicinity of the BH, quickly forming a nearly circular accretion disk (Kremer et al. 2019).

Lower BH mass in the micro-TDE case results in a highly super-Eddington accretion that can exceed the Eddington rate $\dot{M}_{\rm Edd} \equiv L_{\rm Edd}/c^2 = 2.6 \times 10^{-9} M_{\rm BH}\ {\rm yr}^{-1}$ by up to a factor of 10^5 (Kremer et al. 2019) or more (Metzger & Stone 2016; Metzger & Fernández 2021; Mummery & Balbus 2021). Here, $L_{\rm Edd}$ is the Eddington luminosity and c is the speed of light. Recent 2D hydrodynamical simulations of hyper-Eddington accretion found strong bipolar outflow, which reduce $\dot{M}$, but they still found the accretion rate to be super-Eddington (Takeo et al. 2020). A large fraction of the disk mass is expected to be blown away as a disk wind. Radiation from the inner accretion disk will escape with a delay, resulting in an extended peak in the light curve (Kimura et al. 2017a, 2017b; Kremer et al. 2019). Further delay in reaching peak luminosity may be expected given that the AGN will surround micro-TDEs with a dense medium. The delay, and even whether the micro-TDE emission can escape the AGN disk, may depend on the mass of the AGN disk and the location of the disruption event within the disk (Perna et al. 2021a). In our fiducial disk model, micro-TDEs are expected mostly in regions around 10^{-4}–10^{-2} pc from the central SMBH, where the disk is ionized and the opacity to scattering is very high, significantly altering the observed emission. However, BHs in the AGN disk are expected to open cavities due to accretion-induced radiation (Kimura et al. 2021), which results in the reduction of opacity, leaving emission from the micro-TDE less affected.

In the case of micro-TDEs in AGNs, a large fraction of the stellar mass remains gravitationally bound to the BH, resulting in a bolometric luminosity of $\lesssim 10^{44}\ {\rm erg\ s^{-1}}$ (Murase et al. 2016; Kremer et al. 2019, 2021). By comparison, the amount of stellar matter available in the case of TDEs depends on the penetration parameter $\beta \equiv R_{\rm t}/R_{\rm p}$. Partial disruption ($\beta \lesssim 1$) is more common, resulting in lower luminosity (Stone et al. 2020). Nonetheless, many observed TDEs have peak luminosities of 10^{43}–$10^{45}\ {\rm erg\ s^{-1}}$ (van Velzen 2018; Wevers et al. 2019; Mummery 2021).

The high accretion rate and low BH mass in micro-TDEs result in high accretion disk temperatures, leading to high X-ray luminosity. In addition, high accretion rate may also result in the launch of relativistic outflows that produce significant γ-ray and X-ray emission (Murase et al. 2016). Such emission would be weaker and longer than typical GRBs, possibly resembling that of ultralong GRBs (Perets et al. 2016). Such γ- and X-ray emission is highly beamed and is therefore only detectable from a fraction of micro-TDEs. Micro-TDE-driven GRBs could be differentiated from other types of GRBs through the identification of a thermal TDE-like counterpart with longer-wavelength observations and possibly directional coincidence with AGNs.

4. SMBHs Too Heavy for TDEs

For SMBHs whose Schwarzschild radius is greater than their tidal radius, stars may be swallowed whole before they can be tidally disrupted. The maximum (nonrotating) SMBH mass capable of producing TDEs, called the Hills mass (Hills 1975), is around $10^8\,M_\odot$ for solar-type stars (Stone et al. 2020). This limit is only weakly dependent on the stellar mass for zero-age main-sequence stars, although it can be greater for off-main-sequence giant stars or for highly spinning SMBHs.

Micro-TDEs in AGNs are not limited by the SMBH mass. Therefore, given the uncertainties in their light curves and spectra, the identification of TDE candidates in AGNs with SMBH mass beyond $10^8\,M_\odot$ may help distinguish micro-TDEs from TDEs.

There have been two identifications of possible TDE emission from AGNs with SMBH mass $M_\bullet > 10^8\,M_\odot$: ASASSN-15lh was an unusually bright transient first discovered by the All-Sky Automated Survey for Supernovae (ASASSN; Shappee et al. 2014) in 2015 at a redshift of $z = 0.232$ (Dong et al. 2016). The spectrum of ASASSN-15lh was suggested to point to a TDE instead of a superluminous supernova origin (Leloudas et al. 2016; Krühler et al. 2018). ASASSN-15lh was found to come from a galactic nucleus with SMBH mass $M_\bullet = 5^{+8}_{-3} \times 10^8\,M_\odot$ (Krühler et al. 2018), which may be a low-luminosity AGN based on its BPT classification (Krühler et al. 2018). This is beyond the Hills mass for solar-type stars, although a highly spinning SMBH in this mass range could still produce a TDE (Kesden 2012). The late-time ($\gtrsim$100 days) light curve and spectrum of ASASSN-15lh could be well explained with a close to maximally spinning SMBH with mass $M_\bullet \sim 10^9\,M_\odot$, although the early light curve and the lack of radio and dim X-ray emission are not understood. Mummery & Balbus (2020) find that the evolving emission requires a low peak temperature. In the case of micro-TDEs, while the disk will have a much higher temperature, lower-temperature emission is expected due to wind reprocessing (Kremer et al. 2021). The peak luminosity of ASASSN-15lh was $L_{\rm peak} \sim 5 \times 10^{45}\ {\rm erg\ s^{-1}}$. This is much higher than the $\lesssim 10^{44}\ {\rm erg\ s^{-1}}$ predicted from analytical micro-TDE models assuming solar-type stars (Leloudas et al. 2016; Kremer et al. 2021), which means that either (i) the analytical models miss some key aspect of the disruption, accretion, or radiation processes; (ii) the disrupted star's mass is much higher than solar; or (iii) the events are not micro-TDEs. The lack of hydrogen and helium features (Dong et al. 2016) also raises the possibility that ASASSN-15lh could be due to the disruption of a Wolf–Rayet star that lost its hydrogen/helium envelope. In this scenario, the emission region needs to remain relatively uncontaminated by the AGN disk gas. Stellar-mass BHs can disrupt Wolf–Rayet stars, while most SMBHs cannot disrupt most Wolf–Rayet stars, making this possibility particularly interesting.

ZTF19aailpwl was a bright ($L_{\rm peak} \sim 10^{45}\ {\rm erg\ s^{-1}}$) transient first observed by the Zwicky Transient Facility (Graham et al. 2019) in 2019 at a redshift of $z = 0.37362$ (Frederick et al. 2021). It originated from an AGN with a reconstructed SMBH mass of $M_\bullet \sim 10^{8.2}\,M_\odot$ (although a mass $<10^8\ M_\odot$ cannot be completely ruled out (Graham et al. 2019). Follow-up observations found that the spectral properties of ZTF19aailpwl are consistent with a TDE (Graham et al. 2019), but also with an AGN flare attributed to enhanced accretion reported by Trakhtenbrot et al. (2019). Its light curve is similar to that of TDEs, with a somewhat longer than usual rise time. For micro-TDEs, such a longer rise time may be possible due to interaction with the disk wind and the low eccentricity of the stellar orbit that makes the encounter less impulsive and the

tidal effects more gradual, compared to the usual SMBH–TDE case.

The reconstructed BH masses for both events beyond the Hills mass point away from TDEs but are consistent with a micro-TDE origin. Nonetheless, TDEs remain a possibility if (i) stars with radii larger than solar, such as red giants, are disrupted and if (ii) the SMBHs have high spin (Kesden 2012).

Micro-TDEs can also occur outside of AGN disks, e.g., in stellar triples hosting BHs (Fragione et al. 2019) or in dense stellar clusters (Kremer et al. 2019; Samsing et al. 2019; Fragione et al. 2021). The micro-TDE rate of these channels is uncertain. These micro-TDEs could also occur in galaxies with SMBH mass above the Hills mass. Observationally, however, these micro-TDE channels will occur far from galactic centers and will not be confined to AGNs. Both ASASSN-15lh and ZTF19aailpwl were localized to galactic centers hosting AGNs, making their non-AGN-assisted micro-TDE origin unlikely.

4.1. Observational Estimate of the Micro-TDE Rate Density from the Heaviest SMBHs

We estimated the micro-TDE rate density from observations. For this, we used the rate density of TDE candidates in galaxies with $M_\bullet \gtrsim 10^8\,M_\odot$, which are difficult to explain with disruption by SMBHs. We used the TDE host galaxy SMBH mass function estimated by van Velzen (2018) based on about two dozen observed TDE candidates. van Velzen (2018) found that the mass function is roughly constant for $M_\bullet < 10^{7.5}\,M_\odot$, while it sharply drops for $M_\bullet > 10^{7.5}\,M_\odot$ (in this high-mass range, they only consider the detection of ASASSN-15lh). Their reconstructed mass function corresponds to a TDE rate of $5^{+8}_{-4} \times 10^{-2}$ $\mathrm{Gpc^{-3}\,yr^{-1}}$ (1σ uncertainty) for $M_\bullet > 10^8\,M_\odot$. Taking into account the mass function of SMBHs in AGNs (Schulze & Wisotzki 2010), we found that about 1% of micro-TDEs occur in AGNs with $M_\bullet > 10^8\,M_\odot$, corresponding to a rate of $\sim 2\,\mathrm{Gpc^{-3}\,yr^{-1}}$.

This estimated rate is significantly lower than our predicted rate of $\sim 170\,\mathrm{Gpc^{-3}\,yr^{-1}}$ from AGNs. One reason for the lower observed rate could be the difficulty in identifying micro-TDEs in AGNs, especially weaker ones. As AGN light curves fluctuate over time and are difficult to model, it is possible that only the brightest micro-TDEs are identified with certainty. This brightness may depend, for example, on the mass of the disrupted star. If only stars with masses $\gtrsim 10\,M_\odot$ can be detected, this by itself reduces the rate density by a factor of ~ 10.

5. Conclusion

We proposed that micro-TDEs occur in AGN disks and found their rate to be about $170\,\mathrm{Gpc^{-3}\ yr^{-1}}$. Such micro-TDEs may be easiest to distinguish from TDEs around SMBHs by focusing on AGN-hosting galaxies in which the central SMBH's mass is too high ($M_\bullet \gtrsim 10^8 M_\odot$) to tidally disrupt solar-like stars. Two such TDE candidates have been reported so far, ASASSN-15lh and ZTF19aailpwl, both among the highest-luminosity TDE candidates.

The observed rate density of TDE candidates from galaxies with $M_\bullet \gtrsim 10^8 M_\odot$ (van Velzen 2018) is below the micro-TDE rate density of $\sim 2\,\mathrm{Gpc^{-3}\,yr^{-1}}$ predicted in this work for AGNs with $M_\bullet \gtrsim 10^8\,M_\odot$ and might be a bright subpopulation. In addition, one candidate (ZTF19aailpwl) occurred in an AGN, while the other (ASASSN-15lh) probably occurred in a weak AGN.

The unique environments in AGN disks are expected to give rise to a wealth of other interesting phenomena, such as the tidal disruption of a star by a neutron star (albeit at a smaller rate of $0.1\,\mathrm{Gpc^{-3}\,yr^{-1}}$), the formation of Thorne–Żytkow objects (Thorne & Zytkow 1975) when a neutron star in the disk is unable to tidally disrupt a stellar companion due to a large stellar radius, the tidal disruption of a neutron star by a BH, the tidal disruption of white dwarfs by stellar-mass BHs, with unique signatures (Maguire et al. 2020), and the accretion-induced collapse of neutron stars (Perna et al. 2021b) and white dwarfs (Zhu et al. 2021). As these phenomena also produce electromagnetic transients, the identification of micro-TDEs will also require differentiation from these possibilities.

Further theoretical and observational work is needed to better understand the spectral and temporal properties of AGN-assisted micro-TDEs, differentiate them from TDEs, and observe them against the background of AGN variability. Promising observational signatures that should be searched for include the following:

1. TDE candidates in AGNs that harbor the heaviest SMBHs with mass $>10^9\ M_\odot$.
2. γ-ray/X-ray transient, or an ultralong GRB, directionally coincident with an AGN.
3. Our results indicate that only an ultra-bright subpopulation of AGN-assisted micro-TDEs may have been detected. Potentially dozens of fainter micro-TDEs may have been observed but remain unidentified. For these cases, the AGN light curve should show unusual flaring activity, e.g., such as those observed by Trakhtenbrot et al. (2019).

The authors would like to thank Bence Kocsis, Christopher Kochanek, and Sjoert van Velzen for useful suggestions. I.B. acknowledges the support of NSF under award PHY-1911796 and the Alfred P. Sloan Foundation. G.F. acknowledges support from NASA grant 80NSSC21K1722. ZH was supported by NASA grant NNX15AB19G and NSF grants AST-2006176 and AST-1715661. H.T. acknowledges support from the Grants-in-Aid for Basic Research by the Ministry of Education, Science and Culture of Japan (HT:17H01102, 17H06360). R.P. acknowledges support from NSF award AST-2006839 and from NASA (Fermi) award 80NSSC20K1570.

ORCID iDs

I. Bartos https://orcid.org/0000-0001-5607-3637
G. Fragione https://orcid.org/0000-0002-7330-027X
Z. Haiman https://orcid.org/0000-0003-3633-5403
S. Márka https://orcid.org/0000-0002-3957-1324
R. Perna https://orcid.org/0000-0002-3635-5677

References

Alexander, T. 2017, ARA&A, 55, 17
Alexander, T., & Hopman, C. 2009, ApJ, 697, 1861
Bartos, I., Kocsis, B., Haiman, Z., & Márka, S. 2017, ApJ, 835, 165
Bellovary, J. M., Mac Low, M.-M., McKernan, B., & Ford, K. E. S. 2016, ApJL, 819, L17
Cantiello, M., Jermyn, A. S., & Lin, D. N. C. 2021, ApJ, 910, 94
Demircan, O., & Kahraman, G. 1991, Ap&SS, 181, 313
Dittmann, A. J., Cantiello, M., & Jermyn, A. S. 2021, ApJ, 916, 48
Dong, S., Shappee, B. J., Prieto, J. L., et al. 2016, Sci, 351, 257

D'Orazio, D. J., & Duffell, P. C. 2021, ApJL, 914, L21
Fragione, G., Leigh, N. W. C., Perna, R., & Kocsis, B. 2019, MNRAS, 489, 727
Fragione, G., Perna, R., & Loeb, A. 2021, MNRAS, 500, 4307
Frederick, S., Gezari, S., Graham, M. J., et al. 2021, ApJ, 920, 56
Funato, Y., Makino, J., Hut, P., Kokubo, E., & Kinoshita, D. 2004, Natur, 427, 518
Gayathri, V., Yang, Y., Tagawa, H., Haiman, Z., & Bartos, I. 2021, ApJL, 920, L42
Gondán, L., Kocsis, B., Raffai, P., & Frei, Z. 2018, ApJ, 860, 5
Graham, M. J., Kulkarni, S. R., Bellm, E. C., et al. 2019, PASP, 131, 078001
Hao, L., Strauss, M. A., Fan, X., et al. 2005, AJ, 129, 1795
Hills, J. G. 1975, Natur, 254, 295
Jermyn, A. S., Dittmann, A. J., Cantiello, M., & Perna, R. 2021, ApJ, 914, 105
Kennedy, G. F., Meiron, Y., Shukirgaliyev, B., et al. 2016, MNRAS, 460, 240
Kesden, M. 2012, PhRvD, 85, 024037
Keshet, U., Hopman, C., & Alexander, T. 2009, ApJL, 698, L64
Kimura, S. S., Murase, K., & Bartos, I. 2021, ApJ, 916, 111
Kimura, S. S., Murase, K., & Mészáros, P. 2017a, ApJ, 851, 52
Kimura, S. S., Murase, K., & Mészáros, P. 2017b, ApJ, 851, 53
Kocsis, B., & Tremaine, S. 2011, MNRAS, 412, 187
Kremer, K., Lombardi, J. C. J., Lu, W., Piro, A. L., & Rasio, F. A. 2022, arXiv:2201.12368
Kremer, K., Lu, W., Piro, A. L., et al. 2021, ApJ, 911, 104
Kremer, K., Lu, W., Rodriguez, C., Lachat, M., & Rasio, F. A. 2019, ApJ, 881, 75
Kroupa, P. 2001, MNRAS, 322, 231
Krühler, T., Fraser, M., Leloudas, G., et al. 2018, A&A, 610, A14
Leloudas, G., Fraser, M., Stone, N. C., et al. 2016, NatAs, 1, 0002
Levin, Y. 2007, MNRAS, 374, 515
MacLeod, M., & Lin, D. N. C. 2020, ApJ, 889, 94
MacLeod, M., Ramirez-Ruiz, E., Grady, S., & Guillochon, J. 2013, ApJ, 777, 133
Maguire, K., Eracleous, M., Jonker, P. G., MacLeod, M., & Rosswog, S. 2020, SSRv, 216, 39
McKernan, B., Ford, K. E. S., Bartos, I., et al. 2019, ApJL, 884, L50
McKernan, B., Ford, K. E. S., Bellovary, J., et al. 2018, ApJ, 866, 66
McKernan, B., Ford, K. E. S., Lyra, W., & Perets, H. B. 2012, MNRAS, 425, 460
McKernan, B., Ford, K. E. S., O'Shaugnessy, R., & Wysocki, D. 2020, MNRAS, 494, 1203
Metzger, B. D., & Fernández, R. 2021, ApJL, 916, L3
Metzger, B. D., & Stone, N. C. 2016, MNRAS, 461, 948
Miralda-Escudé, J., & Gould, A. 2000, ApJ, 545, 847
Miralda-Escudé, J., & Kollmeier, J. A. 2005, ApJ, 619, 30
Mummery, A. 2021, MNRAS, 504, 5144
Mummery, A., & Balbus, S. A. 2020, MNRAS, 497, L13
Mummery, A., & Balbus, S. A. 2021, MNRAS, 505, 1629
Murase, K., Kashiyama, K., Mészáros, P., Shoemaker, I., & Senno, N. 2016, ApJL, 822, L9
Özel, F., & Freire, P. 2016, ARA&A, 54, 401
Pan, Z., & Yang, H. 2021, PhRvD, 103, 103018
Panamarev, T., Shukirgaliyev, B., Meiron, Y., et al. 2018, MNRAS, 476, 4224
Perets, H. B., Li, Z., Lombardi, J. C. J., & Milcarek, S. R. J. 2016, ApJ, 823, 113
Perna, R., Lazzati, D., & Cantiello, M. 2021a, ApJL, 906, L7
Perna, R., Tagawa, H., Haiman, Z., & Bartos, I. 2021b, ApJ, 915, 10
Price, D. J., Wurster, J., Tricco, T. S., et al. 2018, PASA, 35, e031
Samsing, J., Bartos, I., D'Orazio, D. J., et al. 2022, Natur, 603, 237
Samsing, J., Venumadhav, T., Dai, L., et al. 2019, PhRvD, 100, 043009
Schulze, A., & Wisotzki, L. 2010, A&A, 516, A87
Secunda, A., Bellovary, J., Mac Low, M.-M., et al. 2019, ApJ, 878, 85
Shakura, N. I., & Sunyaev, R. A. 1973, A&A, 500, 33
Shappee, B. J., Prieto, J. L., Grupe, D., et al. 2014, ApJ, 788, 48
Sirko, E., & Goodman, J. 2003, MNRAS, 341, 501
Springel, V. 2010, ARA&A, 48, 391
Stone, N. C., Metzger, B. D., & Haiman, Z. 2017, MNRAS, 464, 946
Stone, N. C., Vasiliev, E., Kesden, M., et al. 2020, SSRv, 216, 35
Tadhunter, C., Spence, R., Rose, M., Mullaney, J., & Crowther, P. 2017, NatAs, 1, 0061
Tagawa, H., Haiman, Z., Bartos, I., & Kocsis, B. 2020a, ApJ, 899, 26
Tagawa, H., Haiman, Z., & Kocsis, B. 2020b, ApJ, 898, 25
Takeo, E., Inayoshi, K., & Mineshige, S. 2020, MNRAS, 497, 302
Thorne, K. S., & Zytkow, A. N. 1975, ApJL, 199, L19
Trakhtenbrot, B., Arcavi, I., Ricci, C., et al. 2019, NatAs, 3, 242
van Velzen, S. 2018, ApJ, 852, 72
Wang, Y.-H., Perna, R., & Armitage, P. J. 2021, MNRAS, 503, 6005
Wevers, T., Stone, N. C., van Velzen, S., et al. 2019, MNRAS, 487, 4136
Yang, Y., Bartos, I., Gayathri, V., et al. 2019a, PhRvL, 123, 181101
Yang, Y., Bartos, I., Haiman, Z., et al. 2019b, ApJ, 876, 122
Yang, Y., Gayathri, V., Bartos, I., et al. 2020, ApJL, 901, L34
Zhu, J.-P., Yang, Y.-P., Zhang, B., et al. 2021, ApJL, 914, L19
Zrake, J., Tiede, C., MacFadyen, A., & Haiman, Z. 2021, ApJL, 909, L13